Geology and Three Dimensional Finite Strain Analysis around Annapurna Himal, Central Nepal

Geology and Three Dimensional Finite Strain Analysis around Annapurna Himal, Central Nepal

Kazufumi KAWAMITSU* and Daigoro HAYASHI**

*Environment Assessment Center Co., Akebono 2-23-4, Naha, Okinawa 900, Japan
**Department of Marine Sciences, University of the Ryukyus, Okinawa 903-01, Japan

Abstract

Contoured diagram of crenulation cleavage shows a small circle, axis of which indicates N45°E, E10°. Contoured diagram of minor fold shows also the same small circle as that of crenulation cleavage. Therefore, crenulation cleavage and minor fold were firstly formed in the area and then a flexural slip fold deformed the crenulation cleavage and minor fold. The axis of the flexural slip fold is the same as the axis of the small circle, that is, N45°E, E10°.

The important point obtained by the 3D strain analysis is that the poles of XY plane of strain ellipsoid of 13 gneiss pieces sampled around the area show the same small circle, axis of which indicates N45°E, E10°. The reason why their small circles coincide with together is still an open problem for the future.

Introduction

The surveyed region is located in the north of Pokhara around the Annapurna Himal, Central Nepal as shown in Fig. 1. The previous works of the area have been published by Ohta et al. (1973), Pecher (1977), Pecher and LeFort (1977), Kano (1982) and Arita (1983). The Main Central Thrust (MCT) zone is one of the most important tectonic zones of the Himalayas. The thrust dips gently northwards striking east to west and runs subparallel to the Himalayan range. The paper describes the outline of geology, lithology, and three dimensional (3D) finite strain analysis around the Annapurna Himal, and discusses the relationship between the MCT zone and the finite strain.

Geological Setting

Around the Annapurna area, there are four major tectonic units which are called the Midland zone, Main Central Thrust zone (MCT zone), Himalayan Gneiss zone and Tibetan Tethys zone from south to north. They strike generally N50°–80°W dipping 20°–50° NE (average N75°W, 30°NE) as shown in Fig. 4, going to be younger from south to north.

The Midland zone consists of low grade metamorphosed rocks such as sandstone, quartzite and phyllite. The zone is bounded on the MCT zone by the lower MCT. The lower MCT has not been recognized clearly in the area.

The MCT zone lies between the Himalayan Gneiss zone and Midland zone. Its northern fringe is bordered by the upper MCT and the southern fringe by the lower MCT, respectively. The upper MCT is clearly recognized by the difference of lithofacies, though the very boundary is obscure in our survey. The zone is characterized by low to medium grade metamorphic sheared rocks which are black and

A part of this research was presented at the 97th Annual Meeting of the Geological Society of Japan in Toyama, October 7, 1990
Received: June 11, 1991.

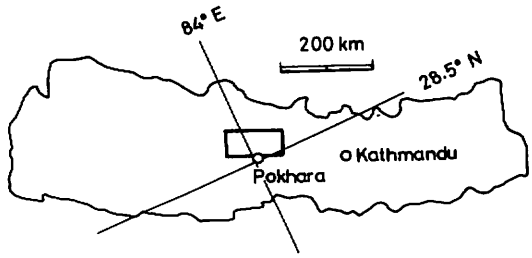

Fig. 1 Index map

green phyllite, quartzite, calcareous rocks and amphibolite.

The Himalayan Gneiss zone consists of various kinds of gneisses and migmatitic gneiss with augen structure. The zone thrusts over the MCT zone along the upper MCT.

The Tibetan Tethys zone is composed of low grade metamorphic quartzite, limestone and mudstone, and overlies the Himalayan Gneiss zone. Their boundaries change gradually and are not recognized directly.

Minor folds are well developed in the Midland and MCT zones. The wavelength of them is about 1–20cm. The contoured diagram of their axes is shown in Fig. 5.

Crenulation cleavages are also well developed in the Midland and MCT zones. The contoured diagram of crenulation cleavages is shown in Fig. 6.

Lithostratigraphy

Midland Group

The group consists of weakly metamorphosed sediments and is overlain by the MCT group. The group is roughly divided into two subgroups; the quartzite and sandstone subgroup, and the sandstone and phyllite subgroup.

The quartzite and sandstone subgroup is mainly composed of quartzite with sandstone interbeds. The quartzite is white in color, including muscovite, biotite and plagioclase. Crenulation cleavages are shown on bedding planes.

The sandstone and phyllite subgroup is mainly exposed in the Midland area. The group consists mainly of biotite bearing black phyllite with quartz veins. Crenulation cleavages and kink folds are seen on the bedding plane.

Main Central Thrust Group (MCT Group)

The group lies between the Himalayan Gneiss group and the Midland group, being bounded by the upper Main Central Thrust at the north, the lower Main Central Thrust at the south. The thickness of the group is 2000m at least. The group has intensely sheared, and consists of the black and green phyllite subgroup, augen gneiss I subgroup, amphibolite subgroup, quartzite subgroup and calcarious phyllite schist subgroup.

The black and green phyllite subgroup is commonly exposed in the area and is composed of biotite–graphite–phyllite, wavy green phyllite and biotite–chlorite phyllitic schist with or without garnet. The phyllitic schist is characterized by wavy micaceous layers with irregularly folded lenticular quartz aggregates. The typical mineral assemblage is garnet–biotite–muscovite–K feldspar–plagioclase–quartz.

The augen gneiss I subgroup is seen at Ulleri along the Kali Gandaki River. The

augen gneiss consists of medium- to coarse-grained minerals. The augen structure comprises K feldspar-porphyroblasts and/or porphyroclasts. The gneiss was called Ulleri augen gneiss by Le Fort (1975). The thickness of the subgroup is about 1000m at least. The representative mineral assemblage is biotite-muscovite-K feldspar-plagioclase-quartz.

The amphibolite subgroup; several amphibolite sheets are placed between the lower and middle parts of the MCT group. The thickness of the sheets is estimated less than 100m. Typical mineral assemblage is hornblend-biotite-quartz-K feldspar.

The quartzite subgroup; a few quarzite layers are placed between the middle horizons of the MCT group along the Kali Gandaki and Modi Khola Rivers. The thickness of the quartzites varies from several hundred to one thousand meters. The colors of the quartzites are white, bluish grey and green. These quartzites are fine- to medium-grained sand size, including thin micaceous layers (1-5mm).

The calcareous phyllite-schist subgroup is exposed close to the upper MCT, and thickness of the subgroup is estimated about 150m.

Himalayan Gneiss Group

The group consists of various kinds of gneisses and thrusts over the MCT group along the upper MCT. The group is, based on the field survey, divided into three subgroups; gneiss I, gneiss II and augen gneiss II subgroups. Structure of these gneisses is generally concordant with that of the upper MCT. Apparent thickness of the group is about 6000m at least.

The gneiss I subgroup; basal part of the Himalayan Gneiss group is composed of the gneiss I subgroup, which is represented by the alternation of pelitic and psammitic gneisses. The pelitic gneiss possesess medium- to coarse-grained minerals, especially garnet which reaches 10mm in diameter, while the psammitic gneiss consists of fine-grained particles. The typical mineral assemblage is garnet-biotite-muscovite-K feldspar-plagioclase-quartz.

The gneiss II subgroup is composed of fine- to medium-grained calc-silicate gneiss and overlies the gneiss I subgroup. The change from the gneiss I to gneiss II subgroup is gradual. Thickness of the subgroup is 2000m at least. The subgroup is usually layered with whitish to greenish quartzose feldsparthic gneissosity which variesfrom 5mm to 20 mm in thickness. Ptygmatic folds are sometimes seen. The typical mineral assemblage is biotite-muscovite-kyanite-calcite-plagioclase-quartz.

The augen gneiss II subgroup, which is composed of migmatitic gneiss with augen structure, occupies the upper part of the Himalayan Gneiss group. The subgroup is developed along the Kali Gandaki and Modi Khola Rivers. The thickness is 400 m at least. The subgroup is characterized by the augen structure which is made of lenticular and euhedral quartz and K feldspar porphyroblasts or aggregates with maximum length 2cm in longitudinal side. The augen is elongated in parallel or subparallel to the foliation. The typical mineral assemblage is biotite-muscovite-K feldspar-quartz.

Tibetan Tethys Group

The group is composed of the crystalline limestone subgroup and the alternation of quartzite and mudstone subgroup. The group overlies the Himalayan Gneiss group

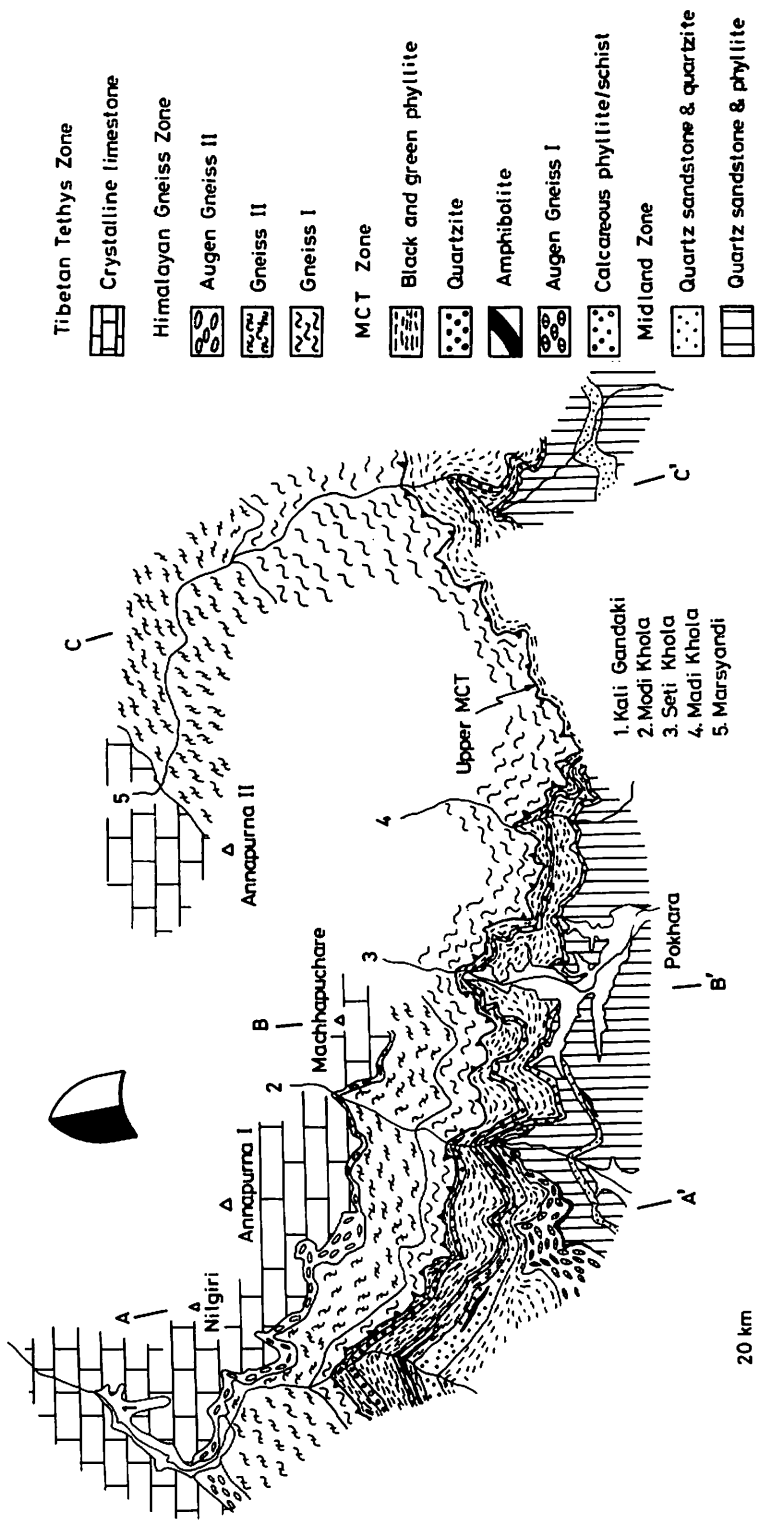

Fig. 2 Geological map.

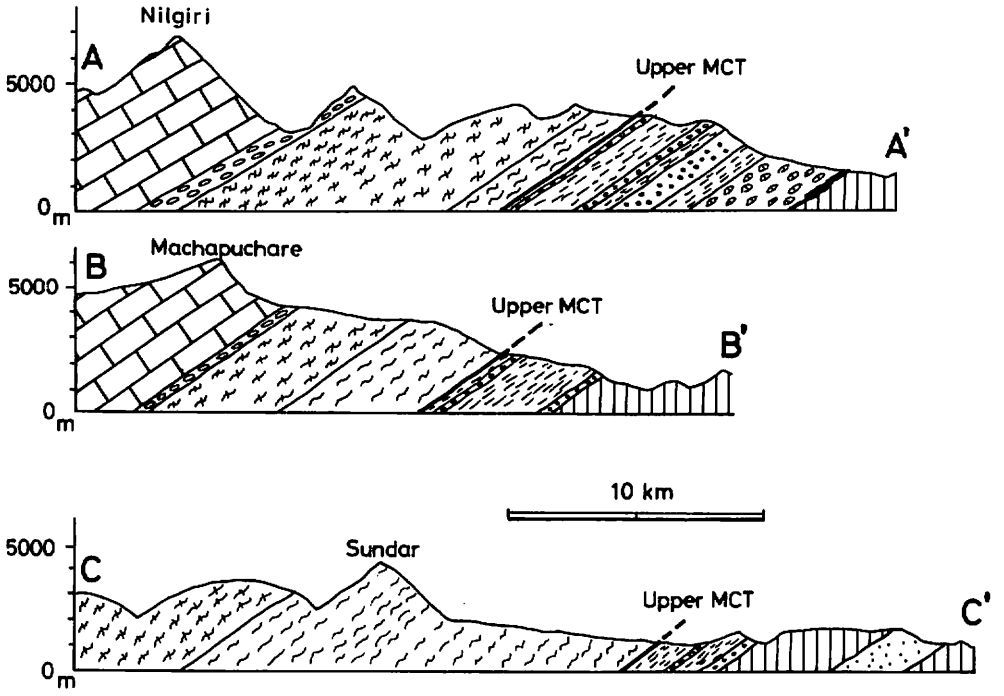

Fig. 3 Geological profile.

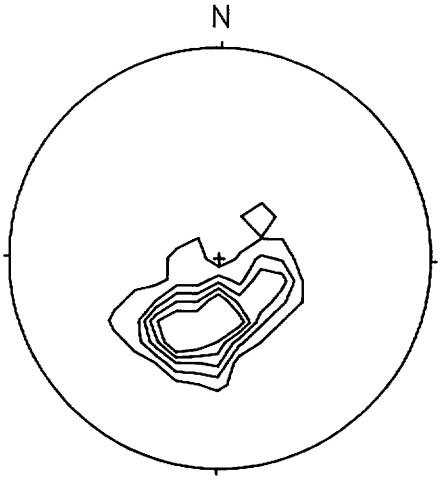

Fig. 4 Contoured S pole diagram of foliation on lower hemisphere. Diagrams are drawn on lower hemisphere hereafter. (155 points; 2-4-6-8-10%).

and seems to be intensely deformed. The wave-length of folding of several kilometers can be recognized. The group is called the Larjung Formation by Bordet et al. (1981). Thickness of the group is more than 2000m.

The crystalline limestone subgroup; basal part of the Tibetan Tethys group is represented by the nonfossiliferous crystalline limestone subgroup. Thickness of the subgroup is 1000m at least.

The alternation of quartzite and mudstone subgroup overlies the crystalline limestone subgroup. The interval of alternation varies from several cm to several m. Thickness of the subgroup is 1000m at least.

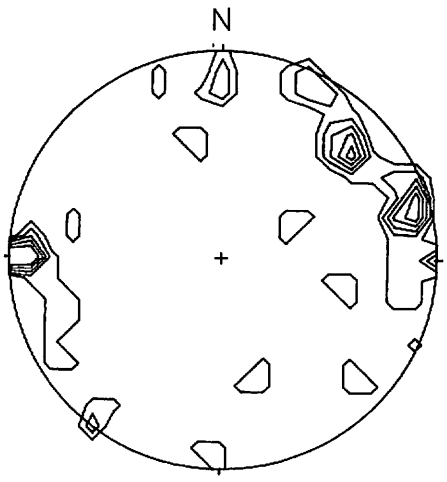

Fig. 5 Contoured fabric diagram of minor fold (35 points; 2-4-6-8-10%).

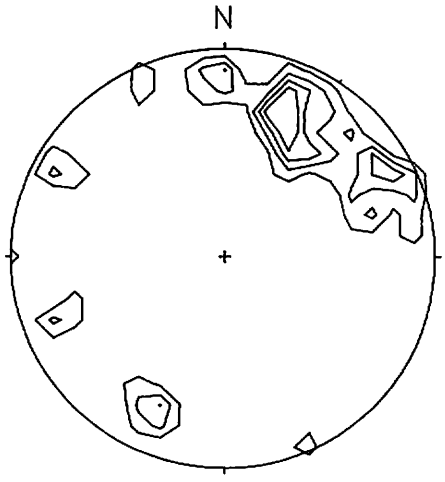

Fig. 6 Contoured fabric diagram of crenulation cleavage (66 points; 2-4-6-8%).

Method of Strain Analysis

Sampling

50 pieces of oriented samples are collected around the southern area of the Annapurna Range, as shown in Fig. 7. Because 13 pieces of them are calcareous schists and gneisses, the other 36 samples are analysed in terms of 3 D finite strain.

Treatment of samples in laboratory

Samples were cut into cubes with edges of approximately 5cm. Each side is named as A, B, and C planes, where these planes share common one apex and form nearly right angles together. Attitudes of A, B and C planes of the oriented samples are described on Table 1. Three rectangular blocks are cut from each cube and refer to A, B and C planes, respectively. Thin sections are made from the rectangular pieces and their photographs are taken through the thin sections. The shapes of 50 to 100 quatz grains are drawn on a transparent sheet, lying on the photograph sheet, respectively. The angle between x and y axes, y and z axes, and z and x axes are indicated on Table 2.

The lower case letters (x, y and z) consist of the coordinate axes, while the upper case letters (X, Y and Z) indicate the principal strain axes of the strain field obtained.

Strain analysis

There are two types of strain analysis, one is called the shape method and the other the orientation method (Hayashi, 1988, 1989). We take the shape method, that is, a shape of quartz grain is assumed as an ellipse which is deformed from its initially elliptic shape.

Shimamoto and Ikeda's method is most suitable for two dimensional strain analysis where calculation is performed by computer, because their method needs merely an algebraic treatment without graphs and other manual operations. On the contrary, if the Rf/ϕ method is taken, it may be formidable for its inevitable interruption of manual work.

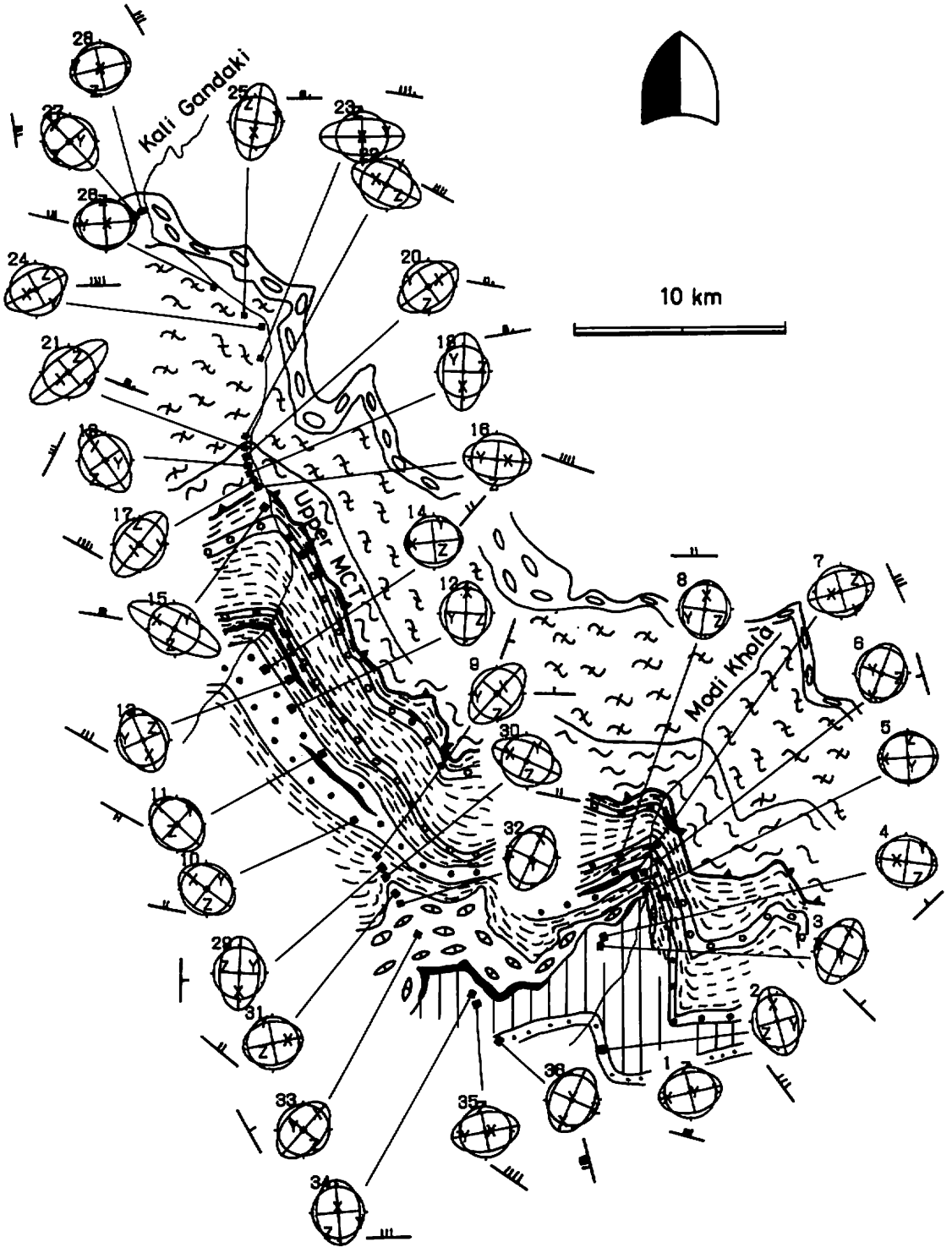

Fig. 7 Distribution of strain ellipsoid.

For 3 D strain analysis, Ramsay's method is used an it seems an only possible way for our study, because we have not known any alternative method, when we use the data which represent three 2D strain values for one oriented sample.

Shimamoto and Ikeda's method for 2D strain analysis was rigorously described in their paper (1976). Ramsay's method for 3 D analysis was presented in his remarkable book (1967).

Results of Strain Analysis

2D strain analysis

Three planes A, B and C of the sample cube are used for the 2D strain analysis. The results of the analysis are then combined each other to make a 3D strain ellipsoid at the sampling point. The results of 2D strain analysis are shown on Table 3. It

Table 1 Attitude of A, B and C planes.

sample number	dip-strike		
	A plane	B plane	C plane
1	N74E62N	N12W81N	N89W29S
2	N56E72S	N22E19N	N38W78N
3	N36E84S	N56W87S	N83E 9N
4	N42W88S	N53E 9N	N48E80S
5	N24E80S	N21W13S	N75W79N
6	N25E87N	N67W86N	N89E 7S
7	N57E74S	N14W43S	N54W49N
8	N57W48N	N52E70S	N22W47S
9	N54E82S	N10W85S	N54W12N
10	N76W70S	N14E86N	N54W21N
11	N23W87N	N70E18S	N64E74N
12	N58E17S	N46E73N	N41W87N
13	N48W36N	N54W57S	N39E89N
14	N18E74S	N59W16S	N77W73N
15	N18E70N	N51W30N	N86W62S
16	N23E78N	N58W61N	N89W35S
17	N37W39S	N71W57N	N25E71S
18	N22W79N	N84W17S	N71E77N
19	N41W69S	N82E30N	N27E66S
20	N68E 8N	N10W85N	N80E81S
21	N79W58N	N24E72S	N45W37S
22	N56W40N	N83W53S	N14E78N
23	N61W37N	N39E82S	N46W55S
24	N14E 8N	N75W89N	N15E82S
25	N77W35S	N87W53N	N 6E81S
26	N47E83S	N40W61S	N66W37N
27	N42E60N	N12E30S	N58W75S
28	N44E82N	N 9W29N	N64W70S
29	N58W89N	N58E 6S	N32E81N
30	N75W16N	N88W76S	N 1E85N
31	N49E10S	N34W87S	N54E82N
32	N39W85S	N66E12N	N53E76S
33	N54W88S	N61E11N	N32E83S
34	N25E76S	N59W72S	N78E23N
35	N52W56S	N80W36N	N30E80S
36	N82W34S	N84E60N	N 1W82N

Table 2 Angle among x, y and z axes (deg). x^y : angle between x and y axes, y^z : angle between y and z axes, z^x : angle between z and x axes

Sample number	angle among x,y,z axes (deg)		
	x^y	y^z	z^x
1	87.9	90.0	89.1
2	88.1	90.2	88.1
3	93.9	90.2	87.7
4	88.6	89.5	89.0
5	87.2	96.8	89.0
6	92.5	90.0	87.8
7	84.5	94.9	91.1
8	87.3	89.7	90.3
9	93.7	86.0	115.2
10	93.7	89.7	88.8
11	92.0	92.1	88.2
12	92.4	89.5	89.4
13	91.8	90.8	93.1
14	88.5	90.1	78.0
15	87.7	92.0	82.2
16	92.1	91.7	92.5
17	84.7	91.3	90.6
18	92.5	83.9	87.6
19	85.2	99.6	87.0
20	89.1	88.4	86.8
21	87.4	89.6	91.4
22	88.1	93.1	89.7
23	89.4	91.2	89.9
24	90.0	90.2	89.1
25	87.4	86.2	87.6
26	94.5	97.8	89.3
27	86.6	90.5	86.5
28	87.5	104.1	100.0
29	86.2	89.6	91.7
30	87.8	88.9	91.2
31	87.2	92.6	88.4
32	87.9	86.9	88.1
33	92.6	93.4	93.2
34	88.9	90.4	91.2
35	92.8	91.5	88.7
36	90.1	87.9	93.4

Table 3 Results of 2D strain analysis.

sample	xy plane				yz plane				zx plane			
number	X	Y	R	Φ (deg)	X	Y	R	Φ (deg)	X	Y	R	Φ (deg)
1	1.29	0.77	1.67	169.52	1.29	0.78	1.66	157.96	1.01	0.99	1.01	199.71
2	1.25	0.80	1.56	173.13	1.08	0.92	1.17	30.87	1.29	0.77	1.67	173.71
3	1.35	0.74	1.83	0.90	1.27	0.79	1.61	128.03	1.11	0.90	1.23	204.88
4	1.32	0.76	1.75	-8.84	1.16	0.87	1.34	86.52	1.19	0.84	1.42	181.52
5	1.03	0.97	1.06	126.31	1.11	0.90	1.24	-18.11	1.10	0.91	1.21	-98.89
6	1.22	0.82	1.48	178.11	1.21	0.83	1.47	190.95	1.04	0.96	1.09	146.30
7	1.19	0.84	1.43	-7.01	1.19	0.84	1.41	173.98	1.16	0.86	1.35	106.70
8	1.18	0.85	1.39	45.44	1.14	0.88	1.30	18.37	1.15	0.87	1.31	113.01
9	1.27	0.79	1.62	162.39	1.33	0.75	1.77	-6.57	1.03	0.97	1.06	126.76
10	1.20	0.83	1.44	156.22	1.12	0.89	1.26	72.33	1.04	0.96	1.09	75.11
11	1.11	0.90	1.24	105.62	1.15	0.87	1.33	37.90	1.05	0.95	1.11	133.85
12	1.12	0.89	1.26	-45.90	1.14	0.88	1.30	84.39	1.25	0.80	1.55	-9.36
13	1.03	0.97	1.07	153.79	1.23	0.81	1.51	235.52	1.32	0.76	1.75	127.19
14	1.13	0.89	1.27	253.59	1.08	0.93	1.16	81.50	1.16	0.86	1.35	-135.67
15	1.24	0.81	1.53	217.06	1.33	0.75	1.76	28.54	1.29	0.77	1.68	255.79
16	1.25	0.80	1.55	-85.64	1.20	0.83	1.44	-52.70	1.20	0.84	1.43	179.73
17	1.32	0.76	1.73	181.61	1.10	0.91	1.21	-74.31	1.24	0.81	1.53	96.43
18	1.17	0.85	1.37	108.48	1.30	0.77	1.69	80.71	1.12	0.89	1.26	-49.52
19	1.32	0.76	1.73	215.33	1.28	0.78	1.64	-120.76	1.20	0.84	1.43	238.33
20	1.36	0.73	1.85	99.40	1.30	0.77	1.69	96.50	1.26	0.80	1.58	97.43
21	1.19	0.84	1.41	98.58	1.30	0.77	1.68	248.13	1.38	0.72	1.91	93.64
22	1.22	0.82	1.49	-8.64	1.19	0.84	1.43	-27.68	1.19	0.84	1.41	95.03
23	1.04	0.96	1.08	120.83	1.36	0.74	1.85	102.83	1.33	0.75	1.77	84.15
24	1.20	0.83	1.44	-72.10	1.15	0.87	1.33	160.76	1.33	0.75	1.78	55.81
25	1.28	0.78	1.63	92.98	1.06	0.95	1.11	-81.59	1.32	0.76	1.74	263.70
26	1.13	0.88	1.28	-16.65	1.07	0.94	1.13	173.20	1.07	0.93	1.15	-84.90
27	1.17	0.86	1.37	105.80	1.11	0.90	1.23	87.70	1.19	0.84	1.42	115.02
28	1.23	0.81	1.52	85.96	1.14	0.88	1.29	113.48	1.07	0.94	1.14	-3.37
29	1.22	0.82	1.48	148.53	1.16	0.86	1.34	-71.43	1.27	0.79	1.62	163.72
30	1.18	0.85	1.39	-38.88	1.26	0.79	1.60	127.29	1.25	0.80	1.56	-34.95
31	1.15	0.87	1.33	182.15	1.27	0.79	1.61	258.45	1.24	0.80	1.55	193.04
32	1.17	0.85	1.38	-170.31	1.22	0.82	1.48	113.94	1.21	0.82	1.48	94.20
33	1.17	0.86	1.36	145.24	1.13	0.89	1.27	83.36	1.27	0.79	1.61	6.78
34	1.21	0.83	1.46	2.00	1.25	0.80	1.56	9.35	1.24	0.80	1.55	128.96
35	1.21	0.83	1.46	223.88	1.14	0.88	1.29	124.36	1.28	0.78	1.64	118.09
36	1.24	0.81	1.53	114.49	1.04	0.96	1.08	-88.07	1.11	0.90	1.23	82.90

should be noticed that the values of X and Y are normalized assuming constant volume (XY= 1).

3D strain analysis

Constructed ellipsoids by the 2D data have two kinds of strain; one is for change of length and the other is for orientation. The former quantity is shown as the Flinn diagram in Fig. 8, whereas the latter is indicated in Figs. 9, 10 and 11. Table 4 shows further the other parameters, which represent shape and intensity of the ellipsoid, i,e., k or K or v and d or D or Es, respectively. The values of X, Y and Z are normalized by the assumption of constant volume.

The Flinn diagram (Fig. 8) shows: (1) Gneiss data are plotted along a line tying a=1. 6~1.7 and b=1.6~1.7. the MCT rock data show a cluster below the line of gneiss data. (2) Intensity of the deformation is quite different between gneiss and MCT rock. (3) 24 samples belong to prolate type and the other 12 samples to oblate type, so that there are meaningful difference in the distribution. (4) Orientations of the principal strain axes show no cluster and no girdle throughout the sampling area (Figs. 9, 10, and 11). Dividing the orientation of Z axes of strain ellipsoid of gneisses from those of MCT rocks, there is a tendency of orientation of Z axes (Fig. 11). The Z axes of gneisses indicate a small circle, whose center trends N45°E plunging 10°.

2D strain on section directed NE to SW

In order to consider the relation of D strain ellipse and foliation on a profile plane

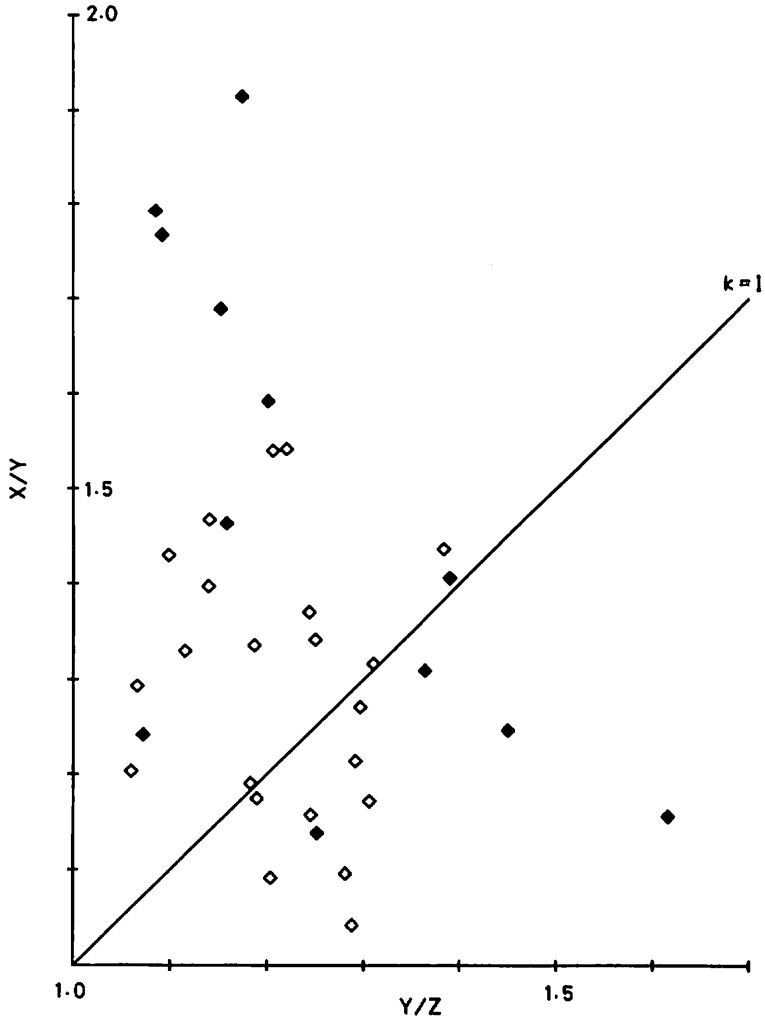

Fig. 8 Flinn diagram.

2, D strain distribution is produced by projecting a strain ellipsoid onto a section A–A' as shown in Fig. 12. Other strain parameters are indicated on Table 5. Strain ellipsoids of 18 samples are projected on a NE–SW section A–A'. XY planes of 13 samples are parallel to the foliation, plane of which dips 35°NW, and the other five samples XY planes are oblique to the foliation.

Discussion

The relations between the fabric patterns and the orientation of the principal axes of strain ellipsoid are interesting subjects. One of the subjects is a problem whether the strain field is consistent with the foliation plane or not. 2D strain feature on the section A–A' will answer this question. It is possible to say from Fig. 12 that XY plane is parallel to the foliation plane. This means that the obtained strain field has

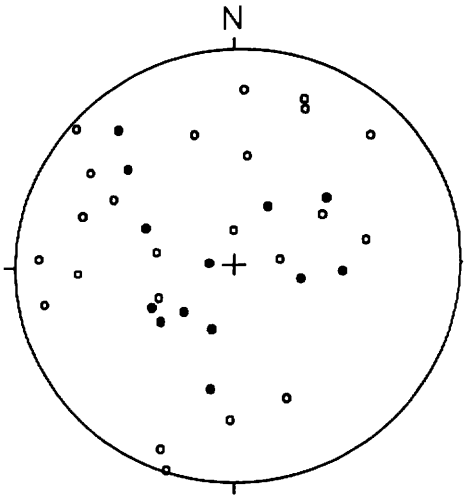

Fig. 9 X axes of strain ellipsoid on Schmidt net.

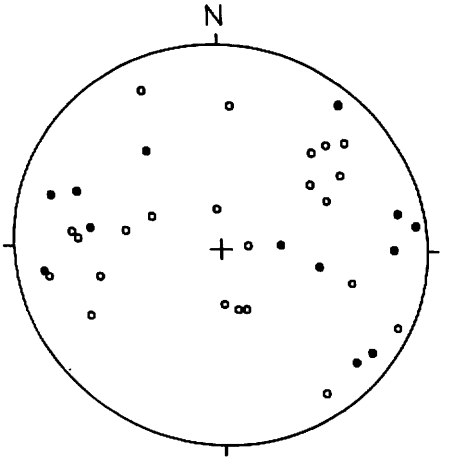

Fig. 10 Y axes of strain ellipsoid on Schmidt net.

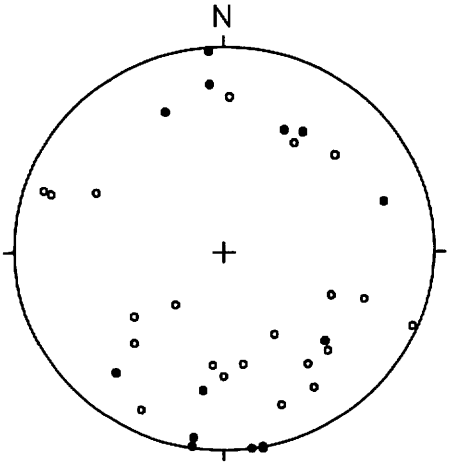

Fig. 11 Z axes of strain ellipsoid on Schmidt net.

reflected the formation of foliation. Three dimensional directions of the pole of XY plane are shown in Fig. 11, since Z axis of strain ellipsoid means the pole of XY plane. If XY plane of strain ellipsoid is parallel to the plane of foliation, the pattern of S pole diagram of foliation measured at the sampling points (Fig. 13) must be identical to that of XY plane of strain ellipsoid. The S pole deagram of foliation shows a cluster, while the XY plane of gneisses shows a small circle. Therefore in terms of three dimension XY plane and foliation of gneisses are not parallel, opposing to the case of two dimension (Fig. 14). The same is supposed for the case of MCT rocks (Fig. 15).

The other interesting points are shown in Figs. 5 and 6. Figure 6 shows that the pattern of crenulation cleavages is a small circle whose axis trends N45°E plunging 10°. Similarly, minor fold pattern is nearly the same small circle as the crenulation cleavages (Fig. 5). The lineation which is initially linear is deformed to a small circle

Table 4 Results of 3D strain analysis.

number	X	Y	Z	Rxy	Ryz	k	d	ε 12	ε 23	K	D	ε s	ν
1	1.215	1.037	.793	1.172	1.308	.559	.352	.159	.268	.592	.312	.305	.257
2	1.327	.968	.778	1.371	1.245	1.514	.444	.315	.219	1.439	.384	.380	-.180
3	1.349	.920	.806	1.467	1.142	3.292	.488	.383	.133	2.889	.405	.379	-.486
4	1.180	1.004	.844	1.175	1.190	.917	.258	.161	.174	.923	.237	.237	.040
5	1.154	.959	.904	1.203	1.061	3.330	.212	.185	.059	3.123	.194	.180	-.515
6	1.186	1.025	.822	1.157	1.246	.640	.292	.146	.220	.665	.264	.261	.202
7	1.311	.977	.781	1.342	1.251	1.364	.424	.294	.224	1.315	.370	.367	-.136
8	1.128	1.033	.858	1.092	1.205	.447	.225	.088	.186	.470	.206	.198	.361
9	1.427	.925	.758	1.542	1.221	2.450	.586	.433	.200	2.167	.477	.458	-.369
10	1.189	.998	.843	1.191	1.184	1.035	.265	.175	.169	1.032	.243	.243	-.016
11	1.213	.938	.879	1.293	1.067	4.354	.301	.257	.065	3.945	.265	.241	-.596
12	1.240	1.021	.790	1.214	1.293	.732	.363	.194	.257	.756	.322	.320	.139
13	1.285	.962	.809	1.336	1.188	1.788	.385	.290	.172	1.682	.337	.330	-.254
14	1.119	1.073	.833	1.042	1.289	.146	.292	.041	.254	.162	.257	.226	.721
15	1.964	.760	.670	2.586	1.134	11.868	1.591	.950	.125	7.575	.958	.832	-.767
16	1.312	1.052	.725	1.247	1.452	.546	.515	.220	.373	.591	.433	.424	.257
17	1.487	.880	.764	1.689	1.153	4.505	.706	.524	.142	3.683	.543	.496	-.573
18	1.505	.852	.780	1.766	1.092	8.286	.772	.569	.088	6.432	.576	.504	-.731
19	1.401	.996	.716	1.406	1.391	1.039	.564	.341	.330	1.033	.475	.475	-.016
20	1.328	1.014	.743	1.310	1.365	.849	.479	.270	.311	.868	.412	.412	.071
21	1.822	.806	.681	2.260	1.184	6.843	1.274	.816	.169	4.824	.833	.745	-.657
22	1.450	.911	.757	1.593	1.202	2.929	.626	.465	.184	2.526	.500	.473	-.433
23	1.627	.850	.723	1.915	1.175	5.233	.932	.650	.161	4.032	.669	.607	-.603
24	1.293	1.118	.692	1.156	1.617	.254	.636	.145	.480	.303	.502	.463	.535
25	1.516	.846	.779	1.792	1.086	9.232	.797	.583	.082	7.087	.589	.513	-.753
26	1.183	.953	.887	1.242	1.074	3.293	.253	.217	.071	3.056	.228	.212	-.507
27	1.354	.925	.798	1.463	1.159	2.907	.489	.380	.148	2.575	.408	.385	-.441
28	1.175	1.032	.824	1.138	1.253	.548	.288	.130	.225	.576	.260	.254	.269
29	1.420	.922	.764	1.540	1.207	2.607	.579	.432	.188	2.293	.471	.450	-.393
30	1.419	.988	.713	1.436	1.385	1.135	.582	.362	.325	1.113	.487	.486	-.053
31	1.155	1.054	.822	1.096	1.283	.340	.298	.092	.249	.369	.265	.249	.461
32	1.306	.935	.819	1.397	1.141	2.824	.421	.334	.132	2.542	.359	.340	-.435
33	1.280	1.007	.776	1.271	1.298	.910	.403	.240	.261	.920	.354	.354	.042
34	1.255	.943	.845	1.330	1.117	2.832	.350	.286	.110	2.587	.306	.289	-.442
35	1.315	.999	.761	1.317	1.311	1.018	.444	.275	.271	1.016	.386	.386	-.008
36	1.310	.916	.833	1.429	1.100	4.308	.441	.357	.095	3.760	.370	.337	-.580

by flexural slip folding. The axis of the small circle coincides with the axis of the flexural slip folding and the radius of the small circle is the angle between the fold axis and the initial lineation. Therefore, the crenulation cleavage and minor fold had firstly been formed, then the flexural slip fold, whose axis is N45°E10°, has deformed the crenulation cleavage and minor fold.

The other remarkable point is that the pole of XY plane of gneisses shows approximately the same small circle as the former two fabrics. The reason is not yet unveiled.

According to Ohta et al. (1973), there are two kinds of lineations in the area. One is the mineral lineation trending NNE to SSW. The other is the minor fold, whose axes stretch east to west. The mineral lineation is older than the minor fold because the mineral lineation was bent by the minor fold. Minor folds existed also as the NE to SW trending lineation in the area and they show the similar small circle to the crenulation cleavage and minor folds which we have studied (Ohta et al., 1973, p.180, Fig. 10 C, S 1. 1', S 2, G 3. 4, S 4).

Table 6 shows symmetry indices for three principal planes of each samples. The symmetry indices show that a sample of number 28 is at least removed from the strain analysis, because its symmetry index shows 0.385 which is the value far from 0.60.

Figure 16 indicates a destribution of strain intensity described by ε_s. The upper MCT cut the iso intensity lines.

References

Arita, K., 1983. Origin of the inverted metamorphism of the Lower Himalayas, central Nepal. *Tectonophysics*, 95:43-60.

Bordet. P., M. Colchen, P., Le Fort, & A. Pecher, 1981. The geodynamic evolution of the Himalaya Ten years of research in Central Nepal Himalaya and some other regions. *In*: Gupta, H. K. & F. M. Delany eds. Zagros•Hindu Kush•Himalaya Geodynamic evolution, Am.

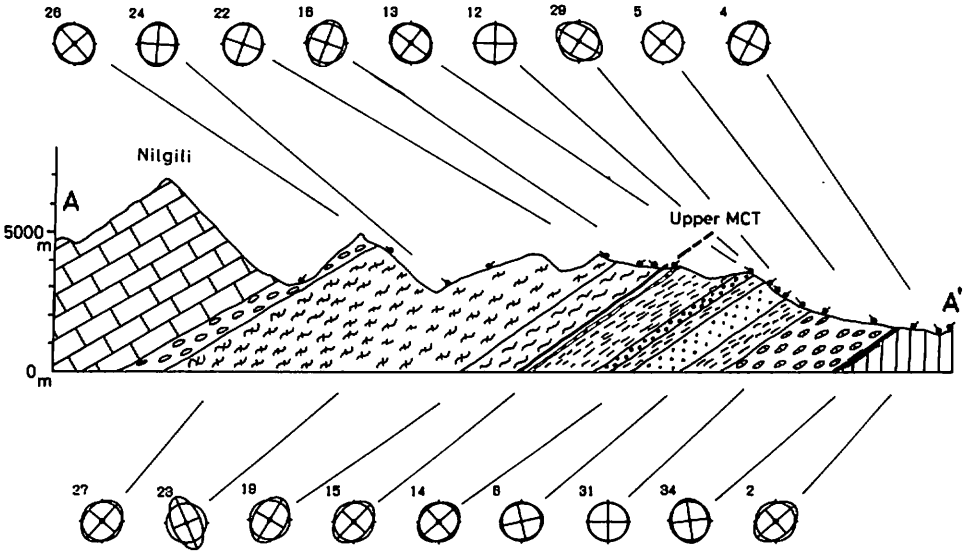

Fig. 12 Profile of strain ellipsoid.

Table 5 2D principal strain on the A-A' profile (Fig. 12).

No.	X	Y	R	Φ(deg)
1	1.088	.919	1.183	-81.0
2	1.240	.807	1.537	39.0
3	1.069	.935	1.143	14.6
4	1.093	.915	1.194	70.2
5	1.020	.980	1.040	88.8
6	1.065	.939	1.134	8.9
7	1.081	.925	1.168	-53.1
8	1.012	.988	1.024	56.1
9	1.168	.856	1.363	55.5
10	1.103	.906	1.217	44.7
11	1.076	.929	1.159	9.0
12	1.069	.935	1.143	-3.4
13	1.134	.882	1.286	-51.7
14	1.115	.897	1.243	32.4
15	1.272	.786	1.619	39.2
16	1.192	.839	1.421	75.4
17	1.071	.934	1.147	88.2
18	1.289	.776	1.661	-40.4
19	1.252	.799	1:566	41.9
20	1.086	.920	1.180	-80.7
21	1.511	.662	2.282	-48.3
22	1.044	.958	1.089	73.6
23	1.353	.739	1.831	-69.8
24	1.107	.903	1.226	86.1
25	1.091	.916	1.191	-55.1
26	1.157	.865	1.338	-86.5
27	1.126	.888	1.269	42.8
28	1.191	.840	1.418	-86.3
29	1.256	.796	1.578	-31.3
30	1.034	.967	1.068	33.6
31	1.070	.935	1.144	-21.6
32	1.056	.947	1.115	18.3
33	1.227	.815	1.505	39.0
34	1.112	.899	1.236	-78.7
35	1.211	.826	1.466	67.4
36	1.143	.875	1.307	-33.0

Geophys. Union, 149-168.

Hayashi, D., 1988. Three dimensional finite strain analysis with reference to Kayo Formation, Kunchan Group, Okinawa-jima. *Jour. Geol. Soc. Japan*, 94: 757-768. (in Japanese with English abstract)

Hayashi, D., 1989. Correction of errors in "Three dimensional finite strain analysis with reference to Kayo Formation, Kunchan Group, Okinawa-jima-Hayashi, 1988". *Ibid.*, 95: 553-558. (in Japanese with English abstract)

Kano, T., 1982. Geology and structure of the Main Central Thrust zone of the Annapurna Range, Central Nepal Himalayas. *Jour. Nepal Geol.Soc., Special Issue*, (2):31-50.

Le Fort, P., 1975. Himalayas : the collided range. *Am.Jour.Sci.*, 275(A): 1-44.

Ohta, Y., C. Akiba, K. Arita, & Y. Maruo, 1973. Pokhara-Gurkha region. *In*: Hashimoto, S.,et al.,eds., Geology of the Nepal Himalayas. Saikon, Tokyo, 159-188.

Pecher, A., 1977. Geology of the Nepal Himalaya: Deformation and petrography in the Main Central Thrust Zone. Colloque Internat. No. 268 Himalaya, Paris 1976, CNRS, vol. Sci. de la Tèrre, 301-318.

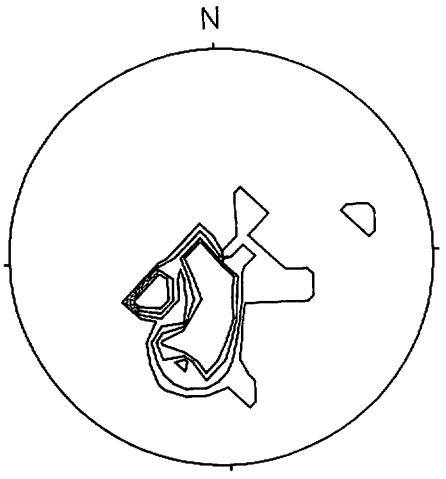

Fig. 13 Contoured S pole diagram of foliation of sample point (36 points; 2-4-6-8%).

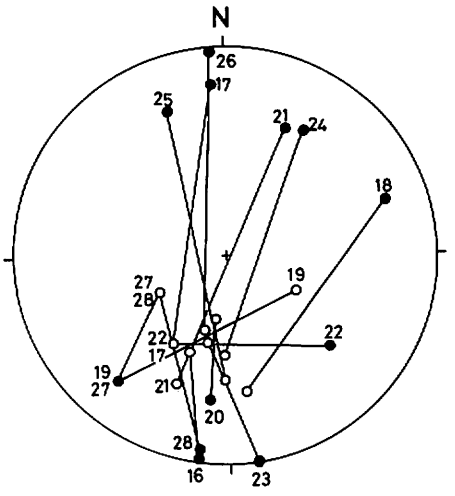

Fig. 14 Comparison of the Z axis (solid circele) with the pole of foliation (open circle) of the Himalayan Gneiss.

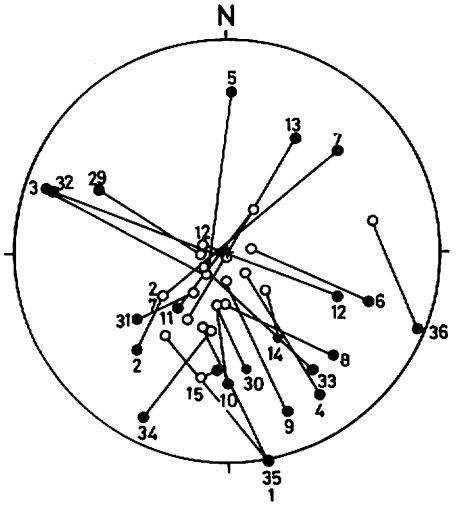

Fig. 15 Comparison of the Z axis (solid circle) with the pole (open circle) of foliation of the MCT rocks.

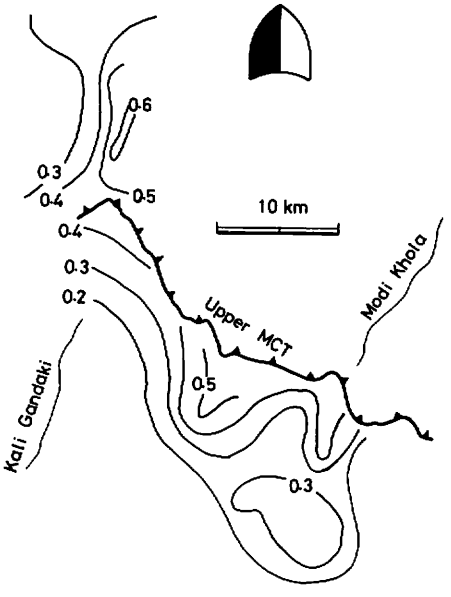

Fig. 16 Contoured strain intensity ε_s map.

Pecher, A. & P. Le Fort, 1977. Origin and significance of the Lesser Himalaya augen gneises. *Ibid.*, 319-329.

Ramsay, J. G., 1967. Folding and fracturing of rocks. 568pp, McGraw-Hill.

Shimamoto, T. & Y. Ikeda, 1976. A simple algebraic method for strain estimation from deformed ellipsoidal objects. 1. Basic theory. *Tectonophysics*, 36: 315-337.

Table 6 Index of symmetry. (sum : sample number, Isym : index of symmetry, ϕ : angle between X axis and strike of examined section.)

No.	xy plane			yz plane			zx plane		
	sum	Isym	Φ (deg)	sum	Isym	Φ (deg)	sum	Isym	Φ (deg)
1	87	.943	-10.9	100	.820	-20.9	100	.960	29.6
2	97	.990	-6.6	80	.875	27.2	76	.974	-6.8
3	97	.845	.1	99	.828	-50.6	100	.760	21.9
4	111	.775	-10.8	102	.922	88.2	129	.961	.3
5	106	.868	-49.3	72	.833	-23.2	59	.712	-89.8
6	100	.940	-3.3	100	.740	7.8	100	.940	-31.4
7	100	.940	-7.0	101	.812	-7.9	101	.832	-71.1
8	95	.758	42.9	102	.961	16.4	90	.911	-65.0
9	65	.923	-18.8	80	.950	-7.1	57	.947	-43.7
10	100	.920	-24.6	81	.963	72.7	89	.989	80.8
11	92	.848	-70.0	89	.966	34.7	87	.966	-45.2
12	87	.828	-44.2	80	.950	85.4	78	.769	-10.4
13	86	.814	-19.9	83	.964	55.1	90	.844	-52.2
14	80	.975	73.7	90	.933	80.1	78	.872	42.0
15	53	.792	34.3	51	.863	28.9	43	.930	75.8
16	85	.824	-84.6	70	.857	-50.9	89	.876	-1.5
17	52	.577	-1.0	43	.930	-71.9	28	.786	-85.6
18	40	.750	-70.4	23	.696	81.2	15	.800	-48.3
19	40	.800	34.7	15	.800	59.0	16	.625	55.1
20	13	.769	-81.7	30	.733	-82.2	24	.917	-83.2
21	30	.867	-79.6	18	.778	67.7	18	.667	-84.5
22	12	.833	-8.5	12	.833	-28.3	14	.857	-83.3
23	13	.769	-60.1	38	.947	-77.2	36	.889	83.9
24	87	.782	-69.7	81	.864	-20.2	69	.957	56.0
25	71	.845	-87.1	74	1.000	-77.1	60	.733	85.0
26	46	.870	-19.3	44	.818	-15.1	45	.800	-77.7
27	22	.727	-71.1	46	.913	87.1	22	.909	-62.6
28	12	.833	87.4	20	.600	-62.3	26	.385	-10.5
29	90	.889	-31.1	81	.914	-69.7	89	.809	-17.6
30	70	.914	-37.7	79	.785	-51.6	80	.850	-34.2
31	72	.861	.9	49	.898	78.5	70	.771	10.7
32	46	.826	6.7	41	.829	-64.0	52	.846	-83.0
33	41	.732	-33.2	20	.800	82.5	45	.844	5.8
34	69	.899	1.0	50	.840	8.4	53	.830	-48.4
35	82	.902	41.8	91	.835	-51.6	85	.706	-60.2
36	60	.900	-65.2	50	.640	-73.7	58	.897	84.2